PHYSICAL REVIEW B **79**, 081405(R) (2009)

Oxygen octahedron reconstruction in the $SrTiO_3/LaAlO_3$ heterointerfaces investigated using aberration-corrected ultrahigh-resolution transmission electron microscopy

C. L. Jia,[1,*] S. B. Mi,[1] M. Faley,[1] U. Poppe,[1] J. Schubert,[2] and K. Urban[1]

[1]*Institute of Solid State Research and Ernst Ruska Centre for Microscopy and Spectroscopy with Electrons, Forschungszentrum Jülich, D-52425 Jülich, Germany*

[2]*Institute of Bio- and Nanosystems and Centre of Nanoelectronic Systems for Information Technology, Forschungszentrum Jülich, D-52425 Jülich, Germany*

(Received 22 September 2008; revised manuscript received 24 November 2008; published 12 February 2009)

We investigate the $LaAlO_3/SrTiO_3$ interface by means of aberration-corrected ultrahigh-resolution transmission electron microscopy allowing us to measure the individual atomic shifts in the interface at a precision of a few picometers. We find that the oxygen octahedron rotation typical for rhombohedral $LaAlO_3$ is across the interface and is also induced in the originally cubic $SrTiO_3$ layer. Octahedra distortion leads to ferroelectricitylike dipole formation in the interface which is in addition modified by cation intermixing.

DOI: 10.1103/PhysRevB.79.081405 PACS number(s): 68.35.−p, 68.37.Og, 73.22.Gk

Perovskite-structured oxides are known for their exceptional variety of physical properties. The report[1] of a high-mobility electron gas at the heterointerface between the two nominally insulating perovskites $LaAlO_3$ (LAO) and $SrTiO_3$ (STO) has stimulated intensive research efforts concerning the physical origin of this intriguing effect and the possibility to derive from it new electronic device applications.[2–5] This has added to the list of particular properties of this interface the observation of ferromagnetism below 1 K (Ref. 6) and of superconductivity below 0.2 K.[7] The effervescent magic source of a seemingly inexhaustible flux of new and surprising properties is provided by a manifold of ways. The cation-oxygen octahedra representing the prominent structural element of perovskites can be modified by, e.g., distortions, rotations, or particular atomic shifts. On the other hand, even small atomic rearrangements as they are expected to occur in interfaces between perovskites of different structure can change dramatically the electronic system.[8,9] High-resolution structural investigations are therefore highly desirable to elucidate the mechanisms behind the observed interface-related properties. Not only that the physical models have to be validated with respect to their structural consequences, all the theoretical approaches by first-principles electronic structure calculations have to start with a suitable structure model[10–13] which, as long as atomic details are not available, is largely constructed based on the perfect (or further simplified) bulk structures. In the light of the versatility of physical properties of perovskites and the complex response to even very small atomic rearrangements, progress in the atomic characterization will help to advance the theoretical modeling of the interfaces.

In the present work we investigate the atomic structure of LaO-TiO_2-type interfaces in epitactic LAO/STO heterostructures by means of aberration-corrected ultrahigh-resolution transmission electron microscopy. Employing the negative-spherical aberration imaging (NCSI) technique[14] we reveal substantial rearrangements of the oxygen octahedra in the interface as well as in the adjacent areas.

STO has cubic perovskite structure [Figs. 1(a) and 1(b)] with a lattice parameter $a=0.3905$ nm. At room temperature LAO has rhombohedral structure [Figs. 1(c) and 1(d)].[15–17] This forms during cooling from a high-temperature cubic structure by rotation of the oxygen octahedra about the $\langle 111\rangle$ axis. LAO is generally described in terms of a pseudocubic structure with a lattice parameter of $a_p=0.3792$ nm. In the following pseudocubic indices will be used as indicated by the subscript "p." With respect to STO the lattice mismatch of LAO is −2.9%.

The LAO/STO multilayer systems used for our measurements were prepared on STO substrates by high oxygen pressure rf sputtering (HOPS) at about 800 °C (Refs. 18 and 19) as well as pulsed laser deposition (PLD) techniques[20] at

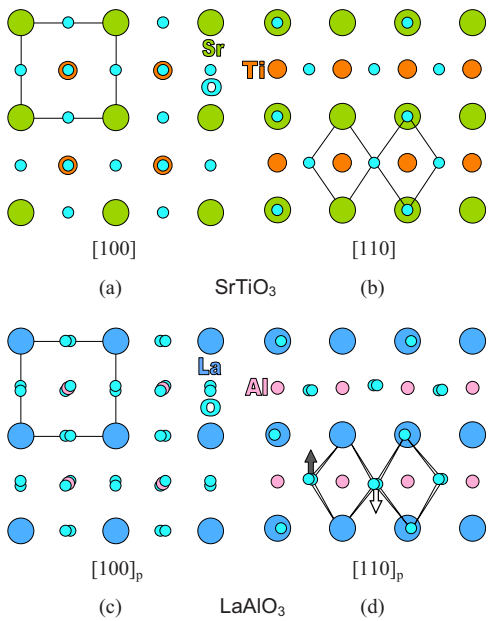

FIG. 1. (Color online) (a) Cubic structure of STO in a projection along the crystallographic [100] direction. A unit cell is lined out. (b) The structure of STO in [110] projection. (c) Rhombohedral LAO in pseudocubic $[100]_p$ projection. (d) Projection of the LAO structure along pseudocubic $[110]_p$. Rotation of two corner-sharing octahedra around the same $[11\bar{1}]_p$ axis but in opposite directions is indicated. Arrows indicate the corresponding shifts of the oxygen atoms out of the $(001)_p$ Al plane.

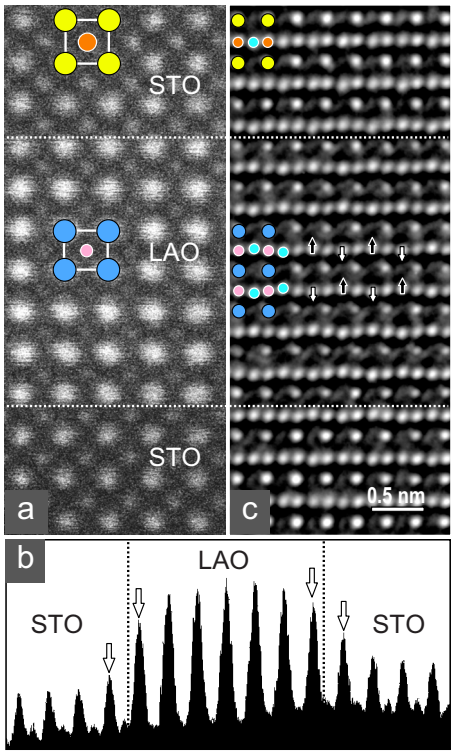

FIG. 2. (Color online) (a) Scanning transmission electron microscopy (STEM) high-angle annular dark field (HAADF) image of a 2.5 nm LAO layer sandwiched between two STO layers taken along the crystallographic [100] direction. The two dotted lines indicate the (001) interfaces. The cubic unit cell in STO and pseudocubic in LAO are lined out: Sr and La atoms are given by large circles and Ti atoms and Al atoms by small circles. (b) Intensity profile of the image averaged over an area along the interfaces. Arrows denote the intensity which changes in comparison with that away from the interfaces. (c) Image taken in a transmission electron microscope (TEM) under NCSI conditions along the [110] direction. Image simulation leads to a defocus value of +5 nm and a sample thickness of 6.6 nm. In LAO the projected shift of the oxygen atoms out of the respective Al-atom rows as a result of oxygen octahedron rotation is clearly visible (arrows).

an oxygen pressure of 1.5 and 2×10^{-3} mbar. We note that the HOPS technique is a low-energy technique producing thin films of very high atomic structural perfection. The results reported here concern the HOPS samples. However no difference was found for the PLD samples. The specimens for high-resolution investigations are carefully prepared to obtain the high quality of the specimens. In particular, the final thinning by ion-beam milling is performed in a stage cooled with liquid nitrogen.

Figure 2 shows two images of a sputter-prepared sample (in cross-sectional preparation) with a 2.5-nm-thick LAO layer sandwiched between two STO layers. Figure 2(a) displays an image obtained by STEM employing the HAADF technique. The viewing direction is parallel to the crystallographic [100] direction of STO. Under HAADF conditions the atoms give bright contrast on a dark background and the intensity increases with the nuclear charge number.[21] As a consequence the intensity decreases from La giving strongest contrast via Sr and Ti to Al giving weakest contrast. Oxygen, due to its low nuclear charge value, does not give enough contrast to be detected. Intensity measurements of the original image allow us to localize the two interfaces [dotted lines in Fig. 2(a)]. Figure 2(b) displays the intensity profiles at the interfaces. As indicated by arrows, increased intensity at the Sr positions next to the interface as well as reduced intensity at the La positions provides evidence for intermixing.

Figure 2(c) is recorded along the $[110]/[110]_p$ direction using the NCSI technique in TEM. Under these conditions the atoms give rise to negative phase contrast and do also appear bright on a dark background.[22] The individual atoms can be clearly recognized; in particular, this refers to the projection of the oxygen octahedra (arrows) and their central Al position (between arrows). Regarding the horizontal -Al-O-Al-O- atom sequence an alternating shift of the oxygen-atom positions upward and downward, respectively, is clearly visible in LAO due to the oxygen octahedron rotation [Fig. 1(d)]. Following the atom positions from the bottom to the top SrO layer and across the interfaces, we find that the alternating up and down shifts of the oxygen atoms with respect to the Ti(Al) positions and the appertaining rotations persist for about three projected unit-cell distances into the STO layers.

Figure 2(c) provides qualitative evidence for the atomic rearrangements. For high-precision measurements we derive from the phase-contrast image intensity distribution the real atomic positions. This is achieved by means of a quantum-mechanical and optical "backward" calculation on a computer whereby image artifacts created by residual lens aberrations and small (unavoidable) tilts away from the fully symmetric Laue orientation can be eliminated. Not only that in this way single-atomic site sensitivity can be achieved, it could be shown that individual atomic shifts can be measured at a precision of a few picometers.[23–25] The data reported in the following have been corrected on this basis.

Figure 3(a) displays the value of the c-axis [001] lattice parameter in STO and the c_p lattice parameter parallel to $[001]_p$ in LAO as a function of vertical distance (in units of c and c_p, respectively) from bottom to top of Fig. 2(c). We find that close to the interfaces (shade lines) the lattice parameter of LAO does not abruptly adopt its central value of 0.375 nm. This, in turn, is by 1% smaller than the bulk value. We also note a small shoulder at both interfaces in the STO layer where c is slightly larger than the bulk value.

Figure 3(b) displays the shift parameter of the oxygen atoms relative to the neighboring Al and Ti atom positions, respectively, as a function of vertical distance. In LAO the values are given by squares for oxygen shifted upward and by circles for oxygen shifted downward. We find that in the center of the LAO layer the moduli, about 10 pm, of the two types of shifts are essentially equal as expected for the ideal structure. Moving downward from LAO into the lower STO layer [left-hand side in Fig. 3(b)] we find that the upward (squares) and downward (circles) shifts of corresponding oxygen positions persist over a distance of about $3c$ into the STO layer. Moving upward from the LAO layer into the upper STO layer [right-hand side of Fig. 3(b)] we find a corresponding behavior. On the right-hand side of Fig. 3(b) negative values for both squares and circles mean that all the oxygen atoms have shifted toward the interface and away

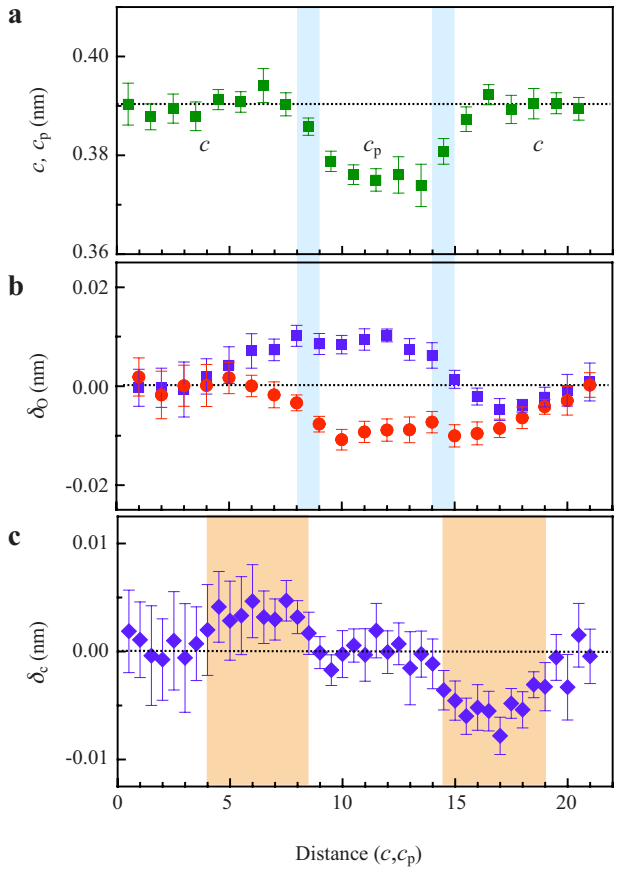

FIG. 3. (Color online) (a) c-lattice parameter in STO and c_p-lattice parameter in LAO as functions of distance (in units of c and c_p, respectively) from a reference plane in the lower STO layer. The vertical shade lines mark the interfaces. (b) The value of the shift parameter δ_O of the oxygen atoms as a function of distance from the reference plane. Squares denote upward shifts and circles denote downward shifts. (c) The value of the shift parameter δ_c of the center of the oxygen octahedra with respect to the appertaining cations. The error bars indicate a 95% statistical confidence level of a Gaussian regression analysis.

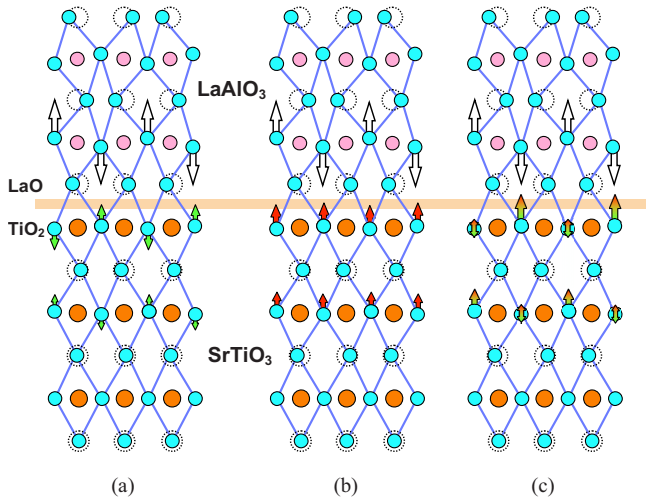

FIG. 4. (Color online) Schematic of octahedron reconstruction at the interface of LAO/STO. (a) Rotation (green/light gray arrows) of rigid octahedra in STO as a result of elastic constraints resulting from the rotation of the oxygen octahedra in LAO. (b) Shift of the oxygen atoms in the TiO_2 planes of STO in the interface area toward the first LaO layer in LAO. The reduced length of the shift arrows increasing distance indicates a reduction in the attraction of the oxygen atoms toward the interface. An equivalent effect is expected from cation intermixing. (c) When the action due to the forces indicated in (a) and (b) is added the shift is enhanced for every second vertical oxygen position while it is diminished in every other.

from the appertaining Ti plane. As a result the center of the octahedron shifts in the direction of the interface. Figure 3(c) displays the measured values of the shifts of the centers of the oxygen octahedra out of the Al plane in LAO (center) and out of the Ti plane in the lower (left-hand side) and upper (right-hand side) STO layers. No shift is, as expected, observed in LAO. On the other hand, an upward shift of 3.5 pm is observed in the lower and a downward shift by about 5 pm in the upper STO layer, i.e., always toward the LAO layer, over a distance of about $5c$. This indicates polarization-dipole formation with the polarization vector pointing away from the LAO layer.

Our measurements provide quantitative evidence for the changes in shape, in rotation angle, and in position of the oxygen octahedra with respect to the cations resulting in polarization-dipole formation. For a more detailed discussion we present in Fig. 4 schematics of the LAO/STO interface where a LaO plane faces a TiO_2 plane (shade line). For clarity the model is simplified with rotation of the octahedra around the [110] projection axis. In the schematic model the rotation angle of the octahedra is enlarged in order to clearly see the octahedron reconstruction across the interface.

Figure 4(a) refers to "rigid" octahedron rotations neglecting for the moment charge effects. In LAO the rotation of a given octahedron is always in the opposite sense with respect to its four corner-sharing neighbors (arrows). At the interface this rotation correlation has to be harmonized with the octahedron arrangement in the STO lattice in which ideally the octahedra are in unrotated form. The rotation mismatch forces the interfacial octahedra to distort also in STO (small green/light gray arrows). Figure 4(b) illustrates the effects induced by electric plane charges. At the interface, disregarding intermixing for the moment, a positively charged $[La^{3+}O^{2-}]$ plane faces a neutral $[Ti^{4+}(O^{-2})_2]$ plane. Considering the atomistic nature of the latter it can be expected that the negatively charged oxygen atoms relax in the electric field upward toward the $[La^{3+}O^{2-}]$ plane (red/gray arrows). This is indeed predicted by theory. It has been found in first-principles calculations that the oxygen in the last TiO_2 layer of STO at the interface is relaxing toward the first LaO layer on the LAO side. As a result oxygen moves out of the respective Ti-atom plane.[11,13,26,27] This leads to ferroelectricitylike distortions of the TiO_6 octahedra with the polarization vector pointing away from the interface as evidenced by our atomic displacement measurements. Figure 4(c) displays the combined effect of rigid octahedron rotation and electric-field-induced atom relaxation. In the first TiO_2 plane below the interface the mechanical force on the first oxygen atom (left-hand side) and the force arising from the electric field are in opposite direction. Depending on the relative magni-

tude of the forces these may compensate each other leading to a zero net shift of the oxygen atom. However, also a small upward or downward shift is possible (symbolized by a small double arrow). This describes the situation for the downward shifts (circles) in the left-hand side of Fig. 3(b). Regarding now the second oxygen in Fig. 4(c), note that both forces are acting in the same direction. This results in a strong upward shift of the oxygen as observed experimentally [Fig. 3(b), left-hand side, squares]. In Fig. 4(c), combining a small upward or downward shift (first oxygen from the left) with a large upward shift (second oxygen) always leads to a net rotation of the oxygen octahedron. Since the charge center of the thus defined pairs of oxygen does not coincide with the respective Ti but rather is shifted upward, the electric dipole character of the interface is maintained. Now let us switch on intermixing. As a result the first LAO plane at the interface will have some La^{3+} substituted by Sr^{2+} with the net effect of a reduction in the positive net charge in this plane. On the other side of the interface La will substitute Sr inducing a positive net charge into the previously neutral $[Sr^{2+}O^{2-}]$ plane. Due to the concentration gradient the corresponding charging effect decreases with distance from the interface. As a consequence the upward shift of the oxygen atoms toward the interface decreases with distance. The effect of this is clearly visible in the experimental data of Fig. 3(b).

At the upper LAO/STO interface [c.f. Fig. 2(c) and right-hand side of Fig. 3(b)] the situation is again described by means of Fig. 4 but upside down. In the case where [cf. Figs. 4(a) and 4(b)] the two forces, mechanical and electrical, have opposite sign the net result is now not a compensation [circles on left-hand STO layer in Fig. 3(b)] but a net downward shift [squares on the right-hand STO layer in Fig. 3(b)]. From this we conclude that the magnitude of the forces and the net result when these are subtracted from each other depend in a subtle way on the local interface quality.

Our study reveals the real atomic structure of the LAO/STO interface. The prominent result is the oxygen octahedron rotation and the TiO_6 octahedra distortion induced by LAO in STO at the interface. Octahedron rotation in the interfacial STO area has not been reported before neither in the experimental nor in the theoretical work. It is well known that, apart from substitutional disorder (likewise not treated as yet in the theoretical models) the lifting of degeneracies by symmetry reduction provides a source for electronic reconstruction effects. We consider the LAO/STO system as just a particularly useful example for the demonstration of complicated structural reconstructions occurring in the interface region of structurally mismatched oxides. These present additional variables into the theoretical efforts to understand the electronic reconstruction intrinsically interrelated with the structural one. On the other hand, perovskite interfaces, due to the proven dramatic effects of subtle changes in structure on the properties of the starting materials, provide us with an excellent example of other systems where an artificially created interface layer of different structure, composition, and related electronic properties displays emergent properties not shown by the "parent" materials.

*c.jia@fz-juelich.de

[1] A. Ohtomo and H. Y. Hwang, Nature (London) **427**, 423 (2004).
[2] S. Thiel *et al.*, Science **313**, 1942 (2006).
[3] M. Huijben *et al.*, Nature Mater. **5**, 556 (2006).
[4] N. Nakagawa, H. Y. Hwang, and D. A. Muller, Nature Mater. **5**, 204 (2006).
[5] C. Cen *et al.*, Nature Mater. **7**, 298 (2008).
[6] A. Brinkman *et al.*, Nature Mater. **6**, 493 (2007).
[7] N. Reyren *et al.*, Science **317**, 1196 (2007).
[8] E. Dagotto, Science **318**, 1076 (2007).
[9] A. Ohtomo, D. A. Muller, J. L. Grazul, and H. Y. Hwang, Nature (London) **419**, 378 (2002).
[10] R. Pentcheva and W. E. Pickett, Phys. Rev. B **74**, 035112 (2006).
[11] M. S. Park, S. H. Rhim, and A. J. Freeman, Phys. Rev. B **74**, 205416 (2006).
[12] S. Gemming and G. Seifert, Acta Mater. **54**, 4299 (2006).
[13] J.-L. Maurice *et al.*, Mater. Sci. Eng., B **144**, 1 (2007).
[14] C. L. Jia, M. Lentzen, and K. Urban, Science **299**, 870 (2003).
[15] S. Geller and V. B. Bala, Acta Crystallogr. **9**, 1019 (1956).
[16] A. M. Glazer, Acta Crystallogr., Sec. A: Cryst. Phys., Diffr., Theor. Gen. Crystallogr. **A31**, 756 (1975).
[17] H. Lehnert, H. Boysen, P. Dreier, and Y. Yu, Z. Kristallogr. **215**, 145 (2000).
[18] U. Poppe *et al.*, J. Appl. Phys. **71**, 5572 (1992).
[19] M. I. Faley *et al.*, Appl. Phys. Lett. **89**, 082507 (2006).
[20] Ch. Buchal *et al.*, Mater. Sci. Eng., B **56**, 234 (1998).
[21] P. D. Nellist and S. J. Pennycook, Ultramicroscopy **78**, 111 (1999).
[22] C. L. Jia, M. Lentzen, and K. Urban, Microsc. Microanal. **10**, 174 (2004).
[23] L. Houben, A. Thust, and K. Urban, Ultramicroscopy **106**, 200 (2006).
[24] C. L. Jia *et al.*, Nature Mater. **7**, 57 (2008).
[25] K. Urban, Science **321**, 506 (2008).
[26] S. Okamoto, A. J. Millis, and N. A. Spaldin, Phys. Rev. Lett. **97**, 056802 (2006).
[27] D. R. Hamann, D. A. Muller, and H. Y. Hwang, Phys. Rev. B **73**, 195403 (2006).